Hindawi
International Transactions on Electrical Energy Systems
Volume 2024, Article ID 9991046, 19 pages
https://doi.org/10.1155/2024/9991046

Research Article

The Multiobjective Control Based on Tolerance Optimization in a Multienergy System

Suliang Ma,[1] **Yaxin Li**,[1] **Yuan Jiang**,[2] **Yiwen Wu**,[1] **and Guanglin Sha**[3]

[1]*School of Electrical and Control Engineering, North China University of Technology, Shijingshan District, Beijing 100144, China*
[2]*School of Automation and Electrical Engineering, University of Science and Technology Beijing, Haidian District, Beijing 100083, China*
[3]*Distribution Technology Center, China Electric Power Research Institute, Haidian District, Beijing 100192, China*

Correspondence should be addressed to Suliang Ma; msl13811581885@ncut.edu.cn

Received 9 December 2023; Revised 2 March 2024; Accepted 28 March 2024; Published 15 April 2024

Academic Editor: Arvind R. Singh

To address the issue of multiobjective control in multienergy systems with diverse operational objectives, a two-stage optimization framework based on expected point tolerance has been proposed in this paper. In the first stage, a single objective function is used for optimization control to obtain the expected point of the multiobjective optimization problem. Then, in the second stage, by defining the allowable deviation between each optimization objective and the expected point, the original multiobjective optimization problem is transformed into a single objective optimization problem solution with tolerance measurement. Finally, in the simulation scene of a multienergy system, it is demonstrated that compared with the optimal results under each single objective method, the proposed method increases power line loss, maximum voltage deviation, new energy consumption, and economy by 2.22, 2.30, 1.02, and 2.45 times, respectively. Compared with the suboptimal results, the proposed method reduces power line loss by 22.26, 1.74, 1.09, and 0.97 times, respectively. Combining the shape of the Pareto frontier, it is demonstrated that the proposed method can comprehensively consider the needs of multiple power optimization objectives for forming a more reasonable and effective system optimization scheduling and also provide a new approach for solving multiobjective optimization problems.

1. Introduction

With the increasing capacity of distributed renewable energy power plants connecting to the grid, the volatility and randomness of renewable energy generation and load consumption pose new challenges to the power balance and stable operation of the grid [1]. Energy storage system (ESS) can effectively accommodate renewable energy generation, improve power quality, and enhance system efficiency. They have been widely applied in modern power systems [2]. However, with the increasing demand for power services and the conflicting optimization objectives of various services, the management and scheduling of renewable energy generation systems and energy storage systems have become increasingly challenging and complex in a multienergy system [3, 4]. The core challenge in further advancing the application of multienergy systems lies in balancing the conflicting demands of various services and establishing a scientific and rational optimization and scheduling strategy. This strategy aims to maximize the fulfillment of diverse optimization requirements and address the multiple objectives effectively.

A significant amount of research has been conducted by domestic and international experts and scholars to address the multiobjective optimization control problem in energy systems, leading to some achievements. For example, in [5], the authors minimize the total generation cost and pollutant emissions of renewable energy systems through two objective functions. This approach enables dynamic economic and emission dispatch control of the system. In [6], a game-theoretic approach is proposed, which utilizes an improved equilibrium coordination algorithm to achieve game

optimization for two operational objectives: wind-storage system generation cost and grid voltage support. This study presents an economic dispatch optimization method for energy storage systems.

Based on existing research, there are three main approaches to address multiobjective optimization. The first approach involves transforming multiple objective functions into a single objective for optimization calculations [7, 8]. For example, in [9], the authors add up the operating costs of different energy sources in a microgrid to convert the multiobjective optimization problem into a single-objective optimization problem. The optimized results obtained through this summation approach lie on the Pareto frontier of the multiobjective optimization, thus achieving optimal energy storage scheduling instructions. In [10], a weighted sum method is used to transform the multiobjective optimization model into a single-objective model, and the influence of weights on the operation cost and lifespan of energy storage batteries is analyzed. Similarly, in [11, 12], a weighted sum approach is utilized to unify objectives such as power loss, load fluctuation, and voltage fluctuation in optimal operation strategies for distribution networks with distributed renewable energy sources. In [13], a model predictive control-based scheduling method for user-side energy storage is proposed, optimizing control with the objective of economic efficiency. In [14], a fuzzy control method is employed to dynamically adjust the weight coefficients of multiple objectives, forming an energy management strategy for hybrid oil-electric systems and achieving global optimal control. The advantage of this approach is that it can yield an effective unique solution. However, the transformation method has a significant impact on the results, and it lacks a characterization of the degree to which the global optimal solution for multiple objectives is approximated. In addition, there is insufficient understanding of the interdependencies between different objectives.

The second approach involves decomposing the multiobjective function into single objectives at different stages for optimization calculations [15–17]. Through iterative interactions between these stages, an optimal value is eventually achieved. For instance, in [18, 19], the day-ahead optimal energy scheduling of a multienergy system is determined in the first stage based on deterministic forecasting information. The second stage involves optimizing and adjusting the energy scheduling instructions based on the dispatch instructions from the first stage. In [20], the first stage employs a real-time pricing strategy to determine the optimal ordered power for loads. In the second stage, a stochastic dynamic interaction between users and suppliers is established by minimizing the difference between actual power consumption and ordered power through real-time incentives, creating a two-layer model. However, in multiobjective optimization problems, there is often a complex coupling relationship between multiple objective functions, which poses significant challenges for the multilevel decomposition process. Moreover, this approach generally results in a trade-off among multiple objective functions, lacking an analysis of the importance level between different objective functions [21].

The third approach involves using swarm intelligence optimization algorithms to compute the Pareto solution set, resulting in a series of nondominated suboptimal solutions [22, 23]. Then, the distribution patterns and influences of these nondominated suboptimal solutions are analyzed [24, 25]. Alternatively, the final recommended value can be obtained by evaluating the suboptimal solutions in the solution set. The drawback of this approach is that the solutions in the solution set are often limited and few in number, and the recommended solution is directly influenced by different evaluation methods. The authors of [26–28] utilize the multiple update strategies (MOMUS) and the nondominated sorting genetic algorithm-II (NSGA-II) to perform multiobjective optimization. The technique for order preference by similarity to an ideal solution (TOPSIS) method is then employed to evaluate the quality of nondominated solutions in the Pareto solution set, ultimately obtaining the recommended solution. The authors of [29] employ a potent symphony orchestra search algorithm (SOSA) to solve nonconvex mixed-integer nonlinear master-slave optimization problems. Then, a conservative fuzzy satisfying method is utilized to select the best compromise solution that meets the economic and flexibility requirements of energy storage systems. In [30], a decomposition-based multiobjective evolutionary algorithm (MOEA/D) is proposed to address the balance between investment in energy storage systems and the internal energy autonomy in active microgrid operations. The authors of [31] utilize the NSGA-II to perform multiobjective optimization for a compressed CO_2 energy storage (CCES) system, considering both its economic and efficiency aspects. The solution closest to the origin in the objective function space on the Pareto front is selected as the final recommended value. In [32], a modified version of the multiobjective sine-cosine algorithm is proposed. Compared to existing methods such as multiobjective grey wolf optimizer (MOGWO), multiobjective slime mould algorithm (MOSMA), nondominated sorting genetic algorithm-II (NSGA-II), and multiobjective particle swarm optimization (MOPSO), this approach is capable of obtaining a better Pareto front. The comparison of the model and method from some existing literature is shown in Table 1.

To address the limitations of the above-mentioned methods, including the lack of representation for the approximation of global optimal solutions in a multiobjective optimization problem and the local optimal problem of the recommended solution based on a Pareto solution set of finite nondominated solutions, a two-stage optimization framework based on the expected point tolerance has been proposed in this paper. The contributions of this paper are as follows:

Table 1: The differences between the optimal scheduling models and methods in the previous related references.

Reference	Components	Objective function	Processing method for multiobjective function
[9]	PV and ESS	Cost of power exchanged with other local microgrids and the grid	Sum of the cost method
[10]	DG, BESS, and microgrid	Determine the lifetime of BESS and the cost of microgrids functioning	Weighted summation method
[12]	DGs and grid	Active power loss, reactive power loss, and the voltage deviation index	Weighted summation method
[18]	DG, PV, ESS, EV, HVACs, and other RLs	Maximizing TVPP's day-ahead and intraday profit in the flexible market	Two-stage adaptive robust optimization
[19]	DN, WIND, PV, ESS, PEMFC, EB, GB, TR, and HS	Carbon trading cost, operational cost, maintenance cost, and rescheduling cost	Two-stage distributionally robust optimization
[21]	DG, renewable energy, ES, and grid	Line loss rate, renewable energy abandonment power penalty item, and ESS residual penalty item	Multistage decoupling structure based on extreme scenario evaluation
[26]	PV, ESS, EV, and grid	Maximizing the profit and minimizing the peak-to-valley difference of the load and loss rate of ESS	MOMUS + TOPSIS
[28]	PV, WIND, BESS, EV, TL, IL, and grid	Maximizing the benefits of GS and maximizing the benefits of LS	NSGA-II + TOPSIS
[32]	DG, ESS, PV, WIND, and grid	Annual energy losses, annual investment, maintenance, and operation costs and reliability	Multi-objective sine-cosine algorithm
This study	PV, wind, DG, and BESS	Line loss, maximum voltage deviation, abandoned amount of new energy, and power generation cost	A two-stage optimization based on expected point tolerance

Note. PV: photovoltaic system; WIND: wind generation; DG: distributed generation; ESS: energy storage system; BESS: battery energy storage system; TVPP: technical virtual power plant; EV: electric vehicle; HVACs: heating, ventilation and air conditioning systems; RLs: responsive loads; DN: distribution network; PEMFC: proton exchange membrane fuel cell; EB: electric boiler; GB: gas boiler; TR: thermal recovery; HS: hydrogen storage tank; TL: transferable load; IL: interruptible load; GS: generation side.

(1) Unlike the existing literature that uses subjective or objective weighting methods to aggregate multiple objective functions or evaluate the Pareto solution set, the proposed two-stage optimization framework in this paper takes a different approach. In the first stage, the optimal values under each objective function are independently calculated multiple times to obtain the expected points of the multiobjective optimization problem, providing a reference for the measurement of optimal solutions. In the second stage, a measurement function is defined to quantify the permissible deviation between feasible solutions and expected points, enabling the optimal solutions to approach the expected points and achieve superior overall performance.

(2) By introducing permissible deviations between feasible solutions and expected points, multiple optimization objective functions are transformed into multiple inequality constraints. Then, the measurement function for permissible deviations is defined to transform the multiobjective optimization problem into a single-objective problem for optimizing the deviations. This approach enables the search for a dominating solution on the Pareto front with the smallest permissible deviation from the expected point, addressing the issue of solution diversity in multiobjective optimization.

The remainder of this paper is organized as follows. In Section 2, a multiobjective optimization problem is analyzed to present the architecture of the proposed method. Then, the mathematical model of a multienergy system with multiple types of objective functions and constraints is established in Section 3. Section 4 analyzes and discusses the optimization performance of the proposed method and the coupling relationships among different objectives. Finally, Section 5 provides the relevant conclusions of this paper and suggests future research directions.

2. Multiobjective Optimization Problems and Solutions

2.1. Multiobjective Optimization Problems. In multiobjective optimization problems, a mathematical model with S objectives can be described as equation (1). In the above equation, $X = [x_1, x_2, \ldots, x_m]$ represents a vector of optimization variables x_i, where $i = 1, 2, \ldots, m$, $f_s(X)$ represents the s-th objective function to be minimized and $g_k(X)$ represents the k-th inequality constraint, while $h_l(X)$ represents the l-th equality constraint and x_i^{lb} and x_i^{ub} denote the lower and upper bounds of the optimization variable x_i, respectively.

$$\underset{\mathbf{X}}{\text{minimize}} \quad F(\mathbf{X}) = [f_1(\mathbf{X}), f_2(\mathbf{X}), \ldots, f_S(\mathbf{X})], \tag{1}$$

$$\text{Subject to} \begin{cases} g_k(\mathbf{X}) \le 0, k = 1, 2, \ldots, K, \\ h_l(\mathbf{X}) \le 0, l = 1, 2, \ldots, L, \\ x_i^{\text{lb}} \le x_i \le x_i^{\text{ub}}, i = 1, 2, \ldots, m. \end{cases} \tag{2}$$

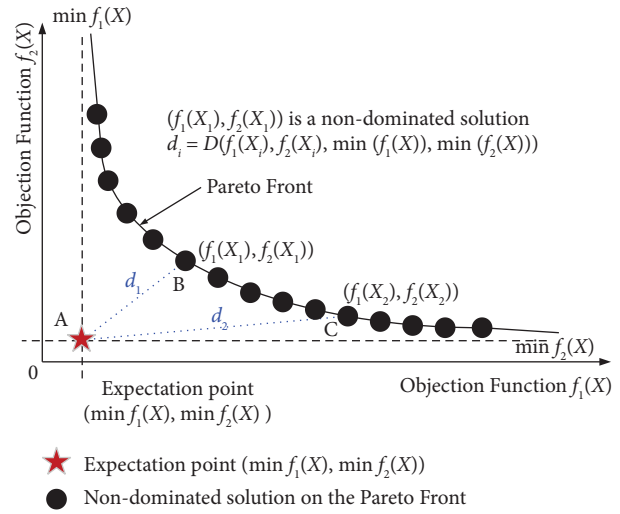

Figure 1: Block diagram for describing multiobjective optimization problems in two objective functions example.

Pareto optimization is a conventional approach to solving the aforementioned multiobjective optimization problems. It involves analyzing the superiority relationships between different solutions to obtain the Pareto-optimal solutions, which are considered nondominated. The relevant definitions regarding Pareto optimality are shown in [32]. However, using Pareto optimization often results in a set of nondominated solutions rather than a single global optimal solution, which can make it challenging to select the best solution. To better illustrate the proposed solution, this paper analyzes the results of Pareto optimality using two optimization objectives as an example, as shown in Figure 1. It can be observed that using Pareto optimization can yield a set of nondominated solutions, forming a convex surface in the multiobjective function space known as the Pareto front. It is worth noting that if this paper independently optimizes each objective, a global optimal point can be obtained in the function space. This global optimal point can be defined as the expected point of the multiobjective optimization problem, as illustrated by point A in the figure. Clearly, in most multiobjective optimization problems, it is not possible to reach this expected point. However, from the figure, it can be seen that the distance between the nondominated solutions on the Pareto front and the expected point is different. This is illustrated by the distances d_1 and d_2 between points B and C on the Pareto front and the expected point A. Therefore, the problem of multiobjective optimization can be transformed into finding the solution in the function space that has the minimum distance to the expected point. This solves the problem of selecting nondominated solutions on the Pareto front. It is worth mentioning that the term "distance" here is just a measure function that describes the proximity between a point in the function space and the expected point. It is not limited to the Euclidean distance as shown in Figure 1.

2.2. A Two-Stage Optimization Process Based on Expected Point Tolerance. Based on the analysis of Figure 1, this paper proposes a two-stage optimization framework based on the expected point tolerance. The objective of this framework is to minimize the deviation between the recommended solution and the expected point by using a measurement function. The specific implementation process is as follows:

Step 1: Under the constraints shown in equation (2), we minimize each objective function $f_s(X)$ to calculate the expected point (min $(f_1(X))$, min $(f_2(X))$, ..., min $(f_s(X))$), as shown in the following equation:

$$\begin{aligned} &\underset{\mathbf{X}}{\text{minimize}} \quad f_s(\mathbf{X}) \\ &\text{Subject to} \quad \begin{cases} g_k(\mathbf{X}) \le 0, k = 1, 2, \ldots, K, \\ h_l(\mathbf{X}) \le 0, l = 1, 2, \ldots, L, \\ x_i^{\text{lb}} \le x_i \le x_i^{\text{ub}}, i = 1, 2, \ldots, m. \end{cases} \end{aligned} \tag{3}$$

Step 2: Based on the single-objective optimization model derived from equation (3), the expected point (min $(f_1(X))$, min $(f_2(X))$, ..., min $(f_s(X))$) is obtained. This paper defines the allowable deviation r_s for a feasible solution on the s-th optimization objective. This allows us to transform multiple optimization objectives into inequality constraints involving the allowable deviation, as shown in the following equation:

$$\frac{f_s(\mathbf{X}) - \min\left(f_s(\mathbf{X})\right)}{\left|\min\left(f_s(\mathbf{X})\right)\right|} \le r_s. \tag{4}$$

Based on equation (4), this paper can transform the multiobjective optimization problem described in equation (2) into an optimization problem involving multiple allowable deviations r_s. The advantages of this transformation include the following: (1) eliminating the biases in optimization results caused by different scales among objective functions, (2) defining a simple and clear measurement function for the allowable deviation r_s, such as a norm, and (3) tailoring the specific value of the allowable deviation r_s according to the specific requirements of practical applications and enabling optimization of the system's optimal results within a specific allowable deviation range for the s-th optimization objective. Taking two norm as an example for the measurement function of the allowable deviation r_s, the above optimization problem can be defined as shown in the following equation:

$$\begin{aligned} &\text{minimize} \sum_{s=1}^{S} r_s^2 = \|\mathbf{r}\|_2^2 \\ &\text{Subject to} \begin{cases} g_k(\mathbf{X}) \le 0, k = 1, 2, \ldots, K, \\ h_l(\mathbf{X}) \le 0, l = 1, 2, \ldots, L, \\ x_i^{\text{lb}} \le x_i \le x_i^{\text{ub}}, i = 1, 2, \ldots, m, \\ f_s(\mathbf{X}) \le |\min\left(f_s(\mathbf{X})\right)| r_s + \min\left(f_s(\mathbf{X})\right). \end{cases} \end{aligned} \tag{5}$$

3. Mathematical Model of Multienergy System

This paper applies the aforementioned methods to a multienergy system consisting of distributed generation, distributed renewable energy, and energy storage system. From the perspectives of grid performance, renewable energy integration, and system economy, four optimization objective functions have been established, including grid line loss, maximum voltage deviation, renewable energy integration, and system generation cost. The calculation formulas for each objective function are shown in Table 2. It is worth noting that in this paper, when establishing the objective function for renewable energy integration, in order to maintain consistency with the other objectives in terms of seeking the minimum value, the negative of the active power output of renewable energy is defined as the optimization objective J_3. Among them, $i_{i,j}(t)$ represents the current flowing from node j to node i at time t, A. $V_i(t)$ represents the voltage at node i at time t, and V_{base} represents the base voltage of the power network, kV. $R_{i,j}$ and $X_{i,j}$ represent the resistance and reactance between node i and node j, respectively, Ω. $P_{\text{DG},i}(t)$ and $Q_{\text{DG},i}(t)$ represent the actual output active and reactive power of the distributed power source at node I at time t, MW and MVar. $P_{\text{ESS\_d},i}(t)$ and $Q_{\text{ESS\_d},i}(t)$ represent the actual discharge active power and reactive power output of the battery energy storage system at node i at time t, MW and MVar. $S_{\text{DG},i}^{N}$ and $P_{\text{ESS},i}^{N}$ represent the rated capacity of the distributed power source and rated power of the battery energy storage system at node i, MW和MW. $P_{\text{New,i}}^{\text{ref}}(t)$ and $P_{\text{New},i}(t)$ represent the maximum active power output and actual active power output of the new energy generation station at the i-th power network node at time t, MW. The new energy generation station primarily refers to photovoltaic (PV) power plants and wind power plants, which are widely used forms of renewable energy with large installed capacities. $k_{1,i}$, $k_{2,i}$, and $k_{3,i}$represent the generation cost coefficients of the distributed power source, ¥/kWh. $k_{4,i}$ and $k_{5,i}$ represent the cost coefficients of the battery energy storage system and the renewable energy station, ¥/kWh. The cost per kilowatt-hour of the battery energy storage system is calculated based on its initial investment cost,

Table 2: Four types of optimization objective functions for multienergy systems.

Meaning of the objective function	Definition of the objective function
Line loss [4, 12]	$\min J_1 = \frac{1}{2}\sum_{t=1}^{T}\sum_{i=1}^{N_b}\sum_{j=1}^{N_b}\left(i_{i,j}^2(t)\times\sqrt{R_{i,j}^2+X_{i,j}^2}\right)$
Maximum voltage deviation [6]	$\min J_2 = \max_{t=1}^{T}\left(\max_{i=1}^{N_b}\left(\mathrm{abs}\left(V_i^2(t)/V_{\mathrm{base}}^2-1\right)\right)\right)$
Abandoned amount of new energy [4]	$\min J_3 = -\sum_{t=1}^{T}\sum_{i=1}^{N_b}\left(P_{\mathrm{New},i}(t)\right)$
Power generation cost [6, 10]	$\min J_4 = \sum_{t=1}^{T}\sum_{i=1}^{N_b}\left(k_{1,i}P_{\mathrm{DG},i}^2(t)+k_{2,i}P_{\mathrm{DG},i}(t)+\ k_{3,i}+k_{4,i}P_{\mathrm{ESS},i}(t)+k_{5,i}P_{\mathrm{New},i}(t)\right)$

maintenance cost, electricity cost, and recovery cost, as well as the amount of discharge throughout its lifecycle. This cost calculation is dependent on the parameters specific to the type of battery energy storage system being considered. In this paper, the distflow optimal power flow (OPF) method [33] has been utilized. Also, the energy storage system is applied to lithium iron phosphate batteries. N_b represents the number of nodes in the power network, T represents the duration of a typical day, and max(·) and abs(·) represent functions that calculate the maximum value and absolute value, respectively.

From the definition formulas of multiple objective functions shown in Table 2, it can be observed that (1) the physical dimensions of the multiple objectives established in this paper are different, making it difficult to directly compare and analyze the importance of each objective. (2) Each objective function is only used as one indicator to evaluate the performance of the multienergy system. This means that in the mathematical modeling of the multienergy system, all objective functions are considered equivalent. Furthermore, it should be noted that the four objective functions mentioned above are only listed to illustrate the methods proposed in this paper. It does not mean that the methods presented in this paper are limited to optimizing only these four objective functions.

In addition to the multiple service objectives mentioned earlier, the optimization and operation control mathematical model of a multienergy system also includes several fundamental requirements for the interaction of energy among different energy sources, the power grid, and loads. These requirements are referred to as constraints. This paper establishes the constraints from the perspective of energy balance and basic physical laws. The constraints include the range of the output power of distributed power sources, the power output and state of charge requirements of energy storage batteries, the actual power output capabilities of renewable energy stations, as well as constraints on active power, reactive power, node voltage, and branch current in the power grid. The definition formulas for all the constraints are shown in Table 3. It can be seen that the operational constraints of a multienergy system are numerous and include many equality constraints, inequality constraints, and second-order cone constraints [34]. The optimization variables consist of continuous and discrete 0-1 variables. Therefore, the optimization problem of a multienergy system is a type of mixed-integer multiobjective programming problem with complex constraints.

Among them, $S_{\mathrm{DG},i}^N$, $P_{\mathrm{DG},i}^{\min}$, $P_{\mathrm{DG},i}^{\max}$, $Q_{\mathrm{DG},i}^{\min}$, and $Q_{\mathrm{DG},i}^{\max}$ represent the rated capacity, lower and upper limits of active power output, and lower and upper limits of reactive power output of the distributed power source at node i, respectively. In this paper, $P_{\mathrm{DG},i}^{\min}=0$, $P_{\mathrm{DG},i}^{\max}=S_{\mathrm{DG},i}^N$, $Q_{\mathrm{DG},i}^{\min}=-S_{\mathrm{DG},i}^N$, and $Q_{\mathrm{DG},i}^{\max}=S_{\mathrm{DG},i}^N$. $C_{\mathrm{SOE},i}(t+\Delta t)$ and $C_{\mathrm{SOE},i}(t)$ represent the energy state of the battery energy storage system at node i at time $t+\Delta t$ and t, respectively, %. Δt represents the time interval in hours, h. $P_{\mathrm{ESS\_d},i}(t)$, $P_{\mathrm{ESS\_c},i}(t)$, and $P_{\mathrm{ESS},i}(t)$ represent the discharge power, charge power, and actual active power of the battery energy storage system at node i at time t, respectively, MW. $\eta_{\mathrm{c},i}$, $\eta_{\mathrm{d},I}$, and $S_{\mathrm{ESS},i}^N$ represent the charging efficiency, discharging efficiency, %, and rated capacity of the battery energy storage system at node i, MWh, respectively. $C_{\mathrm{SOE},i}^L$ and $C_{\mathrm{SOE},i}^D$ represent the lower and upper limits of the energy state of the battery energy storage system at node i, respectively, %. $u_i^c(t)$ and $u_i^d(t)$ represent binary variables indicating the charging and discharging status of the battery energy storage system at node i at time t, with values of 0 or 1. $P_{\mathrm{LOAD},i}(t)$ and $Q_{\mathrm{LOAD},i}(t)$ represent the active power and reactive power demand of the load at node i at time t, MW. $P_i(t)$ and $Q_i(t)$ represent the injected active power and reactive power at node i at time t, respectively, MW. $P_{i,j}(t)$ and $Q_{i,j}(t)$ represent the active power and reactive power flowing from node j to node i at time t, respectively, MW. $I_{i,j}(t)$ represents the magnitude of the current flow $i_{i,j}(t)$ from node j to node i at time t, A^2. $U_i(t)$ and $U_j(t)$ represent the square of the voltage at node i and node j at time t, respectively, kV^2. $U_{\max}$ and $U_{\min}$ represent the square of the upper and lower limits of node voltage, respectively. $I_{\max}$ represents the maximum current flow in the branch. $R_{i,j}$ and $X_{i,j}$ represent the resistance and reactance between node j and node i, respectively, Ω.

4. Case Analysis and Discussion

4.1. Example Parameters. In order to analyze and validate the proposed methods, this paper has considered an IEEE33 distribution network [34] with the integration of two photovoltaic stations (at nodes 6 and 13), two wind power plants (at nodes 22 and 32), one distributed power source (at node 1), and one lithium-ion battery energy storage station (at node 6), as shown in Figure 2. Figure 3 illustrates the power profiles of the load, PV, and wind power generation during a typical day. Also, Figure 4 represents the distribution of active and reactive power demand at each nod in a typical day [34]. The time

Table 3: The operational constraints for multienergy systems.

Meaning of constraints	Definition of constraints
Distributed power output power range [21]	$\left\|P_{\mathrm{DG},i}(t)\ \ Q_{\mathrm{DG},i}(t)\right\| \le S^{\mathrm{N}}_{\mathrm{DG},i}$
Distributed power generation active power output range [12]	$P^{\min}_{\mathrm{DG},i} \le P_{\mathrm{DG},i}(t) \le P^{\max}_{\mathrm{DG},i}$
Distributed power source reactive power output range [12]	$Q^{\min}_{\mathrm{DG},i} \le Q_{\mathrm{DG},i}(t) \le Q^{\max}_{\mathrm{DG},i}$
New energy output active power output range [4]	$0 \le P_{\mathrm{New},i}(t) \le P^{\mathrm{ref}}_{\mathrm{New},i}(t)$
State of charge of energy storage batteries [6]	$C_{\mathrm{SOE},i}(t+\Delta t) = C_{\mathrm{SOE},i}(t) - (P_{\mathrm{ESS\_d},i}(t)/\eta_{\mathrm{d},i} + P_{\mathrm{ESS\_c},i}(t) \times \eta_{\mathrm{c},i}) \times \Delta t \times 100/S^{\mathrm{N}}_{\mathrm{ESS},i}$
Initial state of charge of battery energy storage system [3, 5]	$C_{\mathrm{SOE},i}(0) = C_{\mathrm{SOE},i}(T) = C^{\mathrm{init}}_{\mathrm{SOE},i}$
Charging and discharging power of battery energy storage system [4]	$P_{\mathrm{ESS},i}(t) = P_{\mathrm{ESS\_d},i}(t) + P_{\mathrm{ESS\_c},i}(t)$
Range of state of charge for battery energy storage system [3, 5]	$C^{\mathrm{L}}_{\mathrm{SOE},i} \le C_{\mathrm{SOE},i}(t) \le C^{\mathrm{U}}_{\mathrm{SOE},i}$
Range of discharge power for battery energy storage system [3, 5]	$0 \le P_{\mathrm{ESS\_d},i}(t) \le u^{\mathrm{d}}_i(t) \times P^{\mathrm{N}}_{\mathrm{ESS},i}$
Charging power range of battery energy storage system [3, 5]	$-u^{\mathrm{c}}_i(t) \times P^{\mathrm{N}}_{\mathrm{ESS},i}(t) \le P_{\mathrm{ESS\_c},i}(t) \le 0$
Charge and discharge flag variables [3, 6]	$u^{\mathrm{c}}_i(t) + u^{\mathrm{d}}_i(t) \le 1 \quad u^{\mathrm{c}}_i(t) = 0 or 1 \quad u^{\mathrm{d}}_i(t) = 0 \mathrm{or} 1$
Distributed power output power range [4]	$\left\|P_{\mathrm{ESS},i}(t)\ \ Q_{\mathrm{ESS},i}(t)\right\| \le P^{\mathrm{N}}_{\mathrm{ESS},i}$
Power balance of power grid nodes [6]	$\begin{cases} P_{\mathrm{DG},i}(t) + P_{\mathrm{ESS},i}(t) + P_{\mathrm{New},i}(t) - P_{\mathrm{LOAD},i}(t) = \sum_{j=1}^{N_{\mathrm{b}}} P_{i,j}(t) - \sum_{j=1}^{N_{\mathrm{b}}} I_{i,j}(t) R_{i,j} \\ Q_{\mathrm{DG},i}(t) + Q_{\mathrm{ESS},i}(t) - Q_{\mathrm{LOAD},i}(t) = \sum_{j=1}^{N_{\mathrm{b}}} Q_{i,j}(t) - \sum_{j=1}^{N_{\mathrm{b}}} I_{i,j}(t) X_{i,j} \end{cases}$
The relationship between power, voltage, and current [4, 7]	$\left\| \begin{matrix} 2 \times P_{i,j}(t) \\ 2 \times Q_{i,j}(t) \\ I_{i,j}(t) - U_i(t) \end{matrix} \right\|_2 \le (I_{i,j}(t) + U_i(t))$
Ohm's law [18]	$U_i(t) = U_j(t) + I_{i,j}(t) \times (R^2_{i,j} + X^2_{i,j}) - 2 \times (P_{i,j}(t) \times R_{i,j} - Q_{i,j}(t) \times X_{i,j})$
Grid voltage and power range [12]	$\begin{cases} U_{\min} \le U_i(t) \le U_{\max} \\ 0 \le I_{i,j}(t) \le I_{\max} \end{cases}$

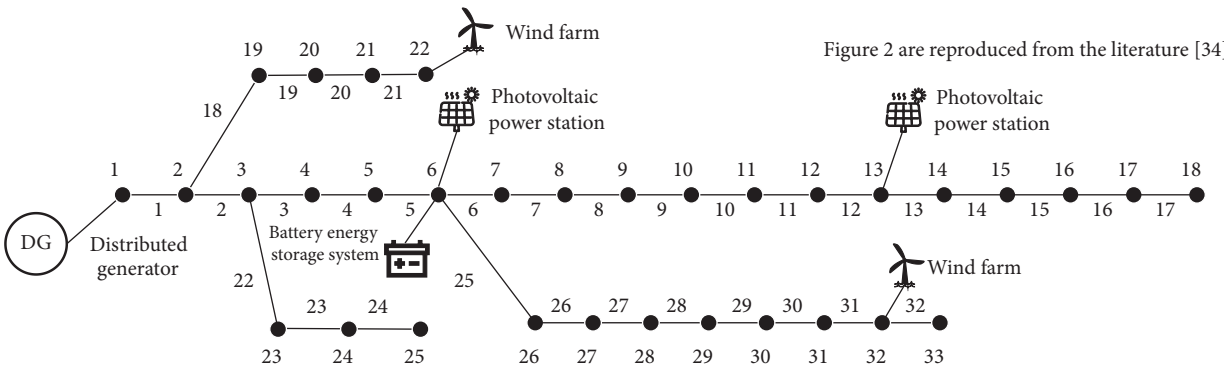

Figure 2: Network topology of IEEE33 system with DG, wind farm, PV station, and BESS.

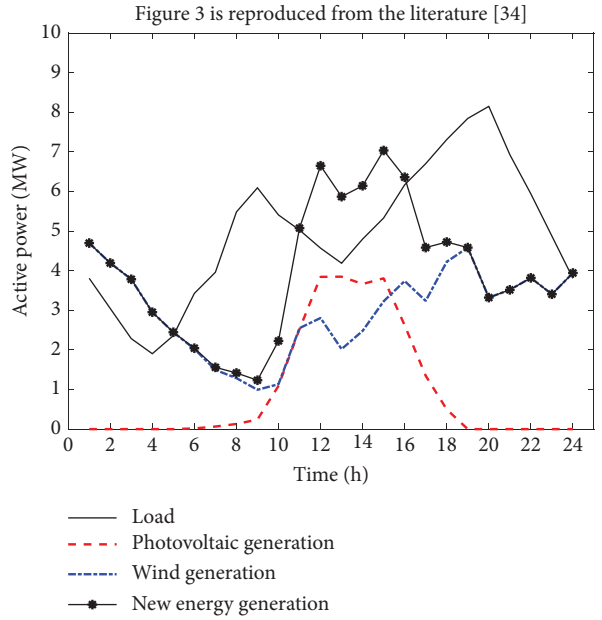

Figure 3: PV, wind power, and load output power curve under a typical day.

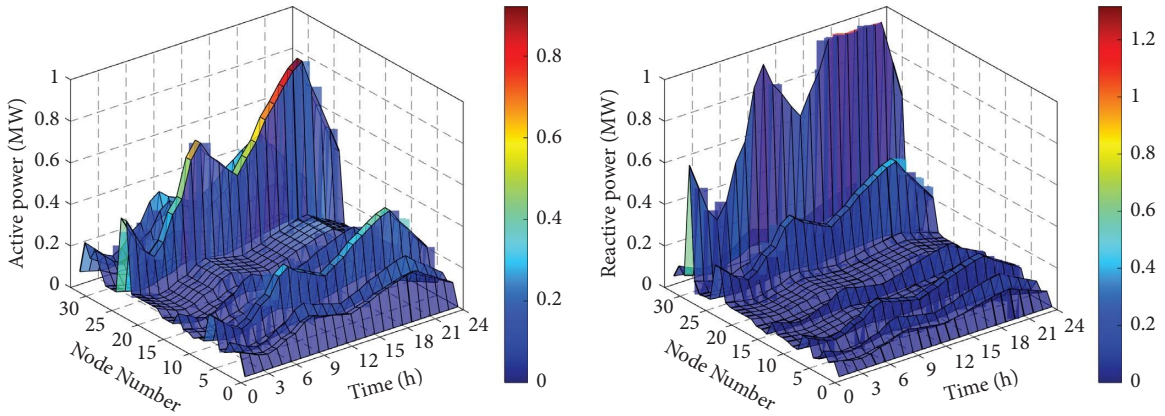

Figure 4: The active and reactive power of loads on 33 nodes at different times.

interval Δt is set to 1 hour, and the duration of the typical day T is 24 hours. The parameters and simulation conditions of the power grid, distributed power sources, PV stations, wind power plants, and lithium-ion battery energy storage station are presented in Table 4. The simulation environment for this case study is MATLAB 2020a running on a Windows 10 system with 32 GB RAM, an Intel Core i7 CPU with a frequency of 2.3 GHz, and 16 cores. To solve the above optimization

Table 4: Description of simulation parameters.

Parameter	Value
Reference capacity (MW)	10
Line nominal voltage (kV)	12.66
Voltage upper and lower limit range (%)	±10
Maximum current of the line (A)	456
Charging and discharging efficiency (%)	95 and 92
Upper and lower limits of SOE (%)	90 and 10
Initial SOE value (%)	50
Rated power of energy storage system (MW)	3.3
Rated capacity of energy storage system (MWh)	13.2
Cost per kWh of energy storage system (¥/kWh)	0.574
Rated power of distributed power sources (MVA)	10
Distributed power generation cost coefficient k_1 (¥/kWh)	40000
Distributed power generation cost coefficient k_2 (¥/kWh)	650
Distributed power generation cost coefficient k_3 (¥)	8
Photovoltaic installed capacity of node #6 (MW)	4
Photovoltaic installed capacity of node #6 (MW)	2
Cost of photovoltaic kWh at nodes #6 and #13 (¥/kWh)	0.293
Wind power installed capacity at node #22 (MW)	3
#32 node wind power installed capacity (MW)	2
Wind power cost per kilowatt hour at nodes #22 and #32	0.3

problem, a mathematical programming solver CPLEX that was developed by IBM has been adopted.

From Figure 2 and Table 4, it can be observed that in the simulation, the PV and wind power generation are dispersedly integrated at four different nodes. The total installed capacity of the renewable energy sources is 11 MW, slightly larger than the rated power of the power sources and the apparent power of the loads. This highlights the challenge of accommodating high penetration levels of renewable energy in the power grid. Particularly, from Figure 3, it can be seen that the load demand is relatively high. During the period from 5 AM to 11 AM and from 4 PM to 12 AM, the output power of the renewable energy sources is insufficient to meet the load demand, and the generators supply the active and reactive power. During the period from 1 AM to 5 AM and from 12 PM to 3 PM, the output power of the renewable energy sources exceeds the load demand, resulting in curtailment of wind and solar power when no energy storage system is installed. In addition, as shown in Figure 4, the load power exhibits two peak periods in the morning and evening, following the users' consumption pattern. The load at each node has significant differences in active power and reactive power demand, and nodes with high power demand are located far from the generator node, resulting in significant network losses.

4.2. Analysis of System Optimization Control Results. Under the simulation parameters mentioned above, this section compares the proposed methods with the results obtained from single-objective optimization. Table 5 presents the variations in the objective function value under the single-objective optimization in the first stage of the proposed methods. Figures 3 and 4 have illustrated the performance comparison of the multienergy system in terms of power sources, renewable energy, energy storage batteries, and the power grid under different optimization approaches. In Table 5, the reason for J_3 being negative is calculated based on Table 2. The larger the absolute value of the objective function value J_3, the better the performance of that objective.

From Table 5, it can be observed that when optimizing with a single objective, only that specific objective is guaranteed to be optimal, while other objectives may perform poorly and fail to achieve a dominant solution across all objectives. For example, when optimizing with the objective function J_1 as the single objective, the objective function value J_2 is 0.21, at least 10 times larger than the other optimization results. Similarly, when optimizing with the objective function J_2 as the single objective, the objective function value J_3 is −2.9924, more than twice as large as the other optimization results. Therefore, in the control of multienergy systems, it is necessary to consider the needs of various objectives and develop comprehensive optimization and scheduling strategies. Compared to the results of single-objective optimization, the proposed methods in this paper perform suboptimally in terms of all objective function values except for J_4. By comparing the variations of objective function J_2 and J_4, it can be observed that as the objective function value J_2 decreases, the objective function value J_4 increases. This indicates a significant trade-off between reducing grid voltage fluctuations and increasing system generation costs.

Figure 5 illustrates the differences in the generator system, renewable energy system, energy storage system, and grid voltage of the multienergy system under different optimization objectives. In Figure 5(a), which shows the comparison of active and reactive power output of the generator, it can be observed that under the single optimization objective of J_2, the active and reactive power output of the generator is significantly higher than the results of other optimization objectives. This is mainly because the objective function J_2 is designed to reduce grid voltage fluctuations and meet the active and reactive power demand

Table 5: Single objective J_1~J_4 optimization results in the first stage of the proposed method.

	J_1	J_2	J_3	J_4
min J_1	0.0294	0.2100	−5.6129	90167.9471
min J_2	1.9392	0.0027	−2.9924	125350.6774
min J_3	1.4559	0.0108	−9.5580	27508.7962
min J_4	4.1385	0.0261	−8.5573	11584.3200
min $\|r\|_2^2$	0.0654	0.0062	−9.3551	28413.7869

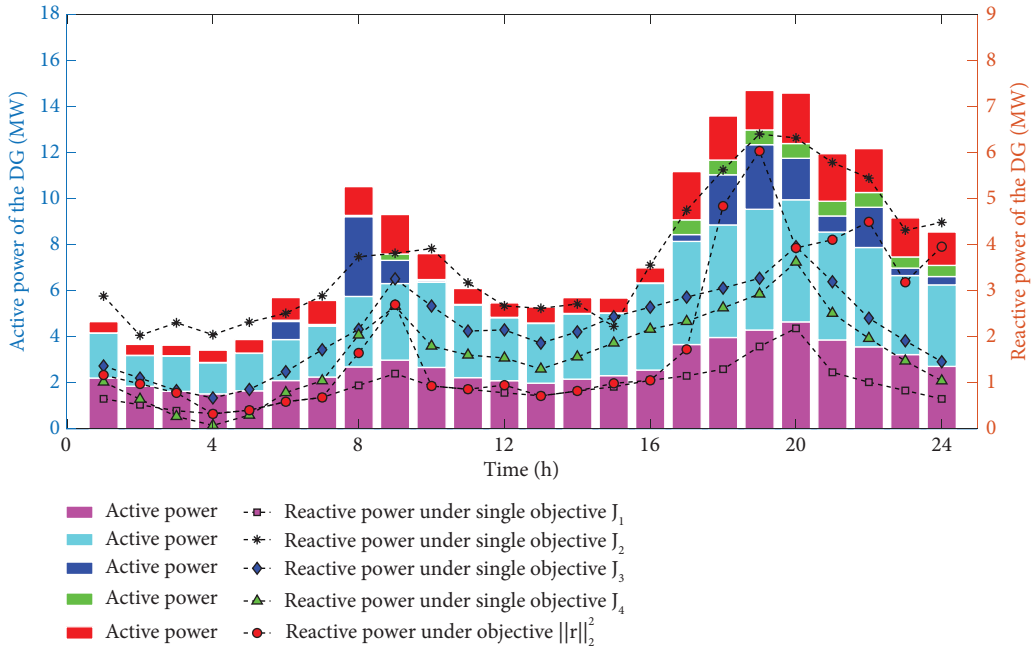

(a)

Figure 5: Continued.

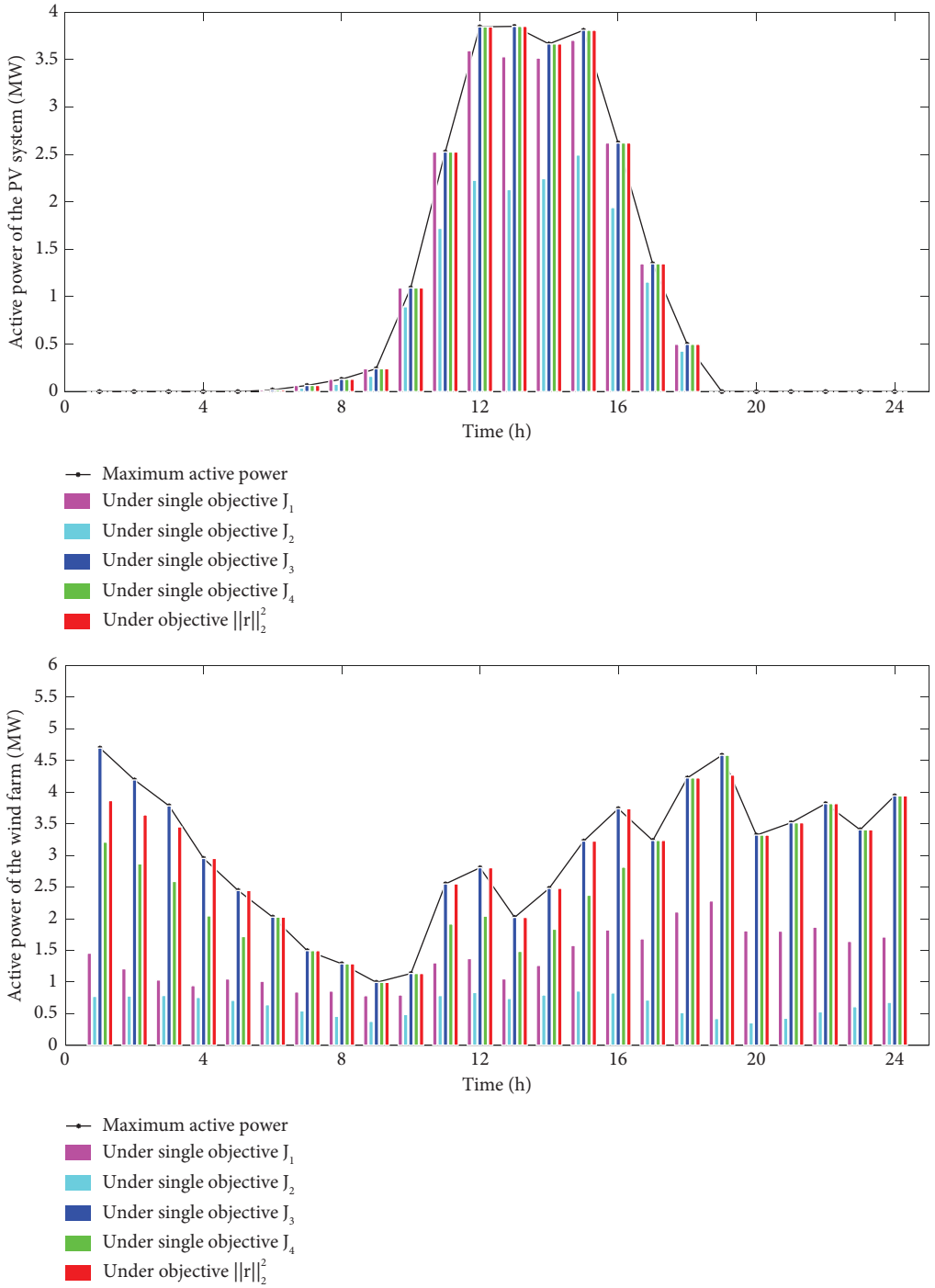

(b)

Figure 5: Continued.

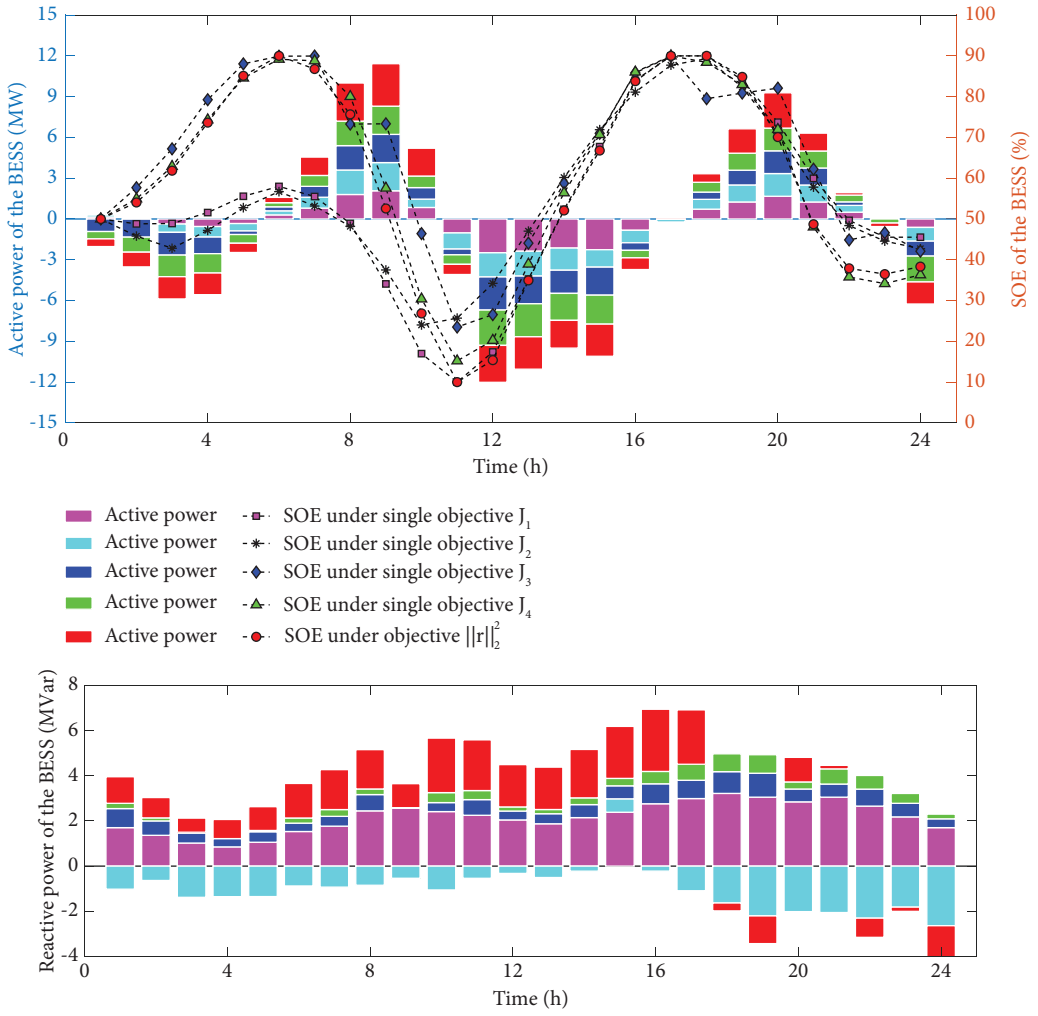

(c)

Figure 5: Continued.

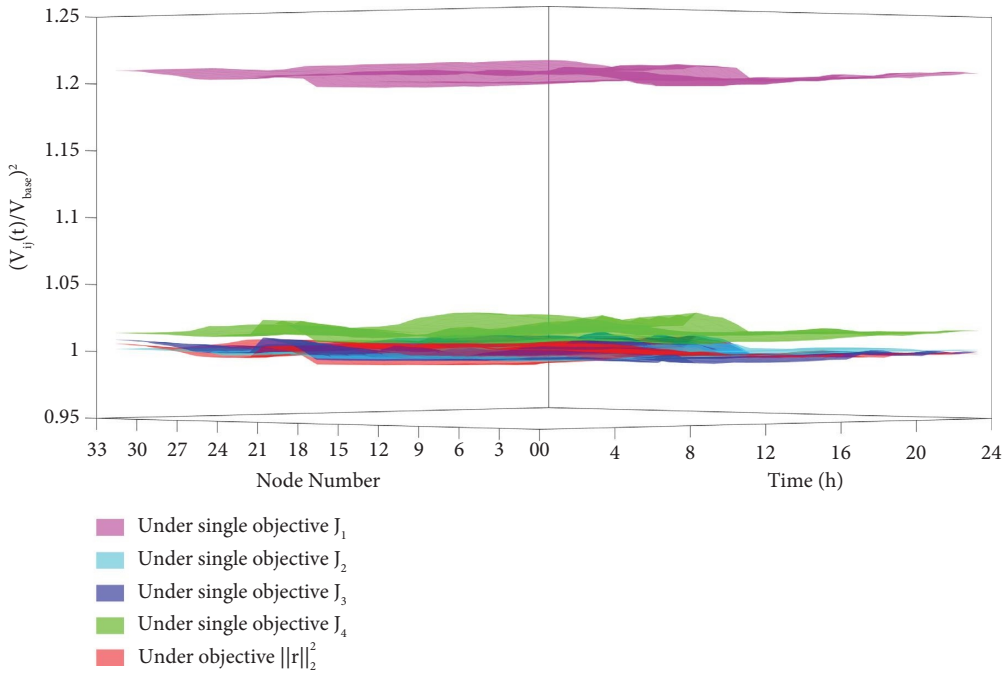

(d)

Figure 5: Comparison results of operational performance of multienergy systems under different optimization objectives. (a) Output active and reactive power from the DG under different optimization objections. (b) Output active power from new energy power stations under different optimization objections. (c) Output active power, reactive power, and SOE from the BESS under different optimization objections. (d) Square of the ratio of grid voltage to reference voltage under different optimization objections.

of the grid load, as shown in Figure 5(b). On the other hand, under the single optimization objective of J_4, the generator's active power output is minimized, and it only provides reactive power to support the grid voltage. This is because J_4 represents the system's generation cost, as shown in formula (9), which is a quadratic function of the actual active power output of the generator. However, in the proposed optimization methods in this paper, the actual power output of the generator lies between these two scenarios, balancing the optimization requirements of objectives J_2 and J_4.

On the other hand, from Figure 5(b), which shows the comparison of actual active power output of the PV and wind power generation systems, it can be observed that under the single optimization objectives of J_1, J_2, and J_4, both PV and wind power generation experience significant and high curtailment, especially for wind power generation. However, under the proposed optimization methods in this paper, the curtailment of renewable energy is significantly reduced. Combined with Figure 5(c), which shows the active power output and energy state of the energy storage battery, it can be seen that between 0 AM and 6 AM, the energy storage system actively charges to absorb the excess wind power generation that exceeds the load demand. Between 6 AM and 11 AM, when the load demand for active power exceeds the maximum output power of renewable energy, the energy storage system discharges to support the load demand. Between 11 AM and 4 PM, due to the higher contribution from PV generation, the renewable energy generation exceeds the load demand, and the energy storage system charges again to prepare for the shortfall in load demand and renewable energy supply resulting from the decrease in PV generation. Figure 5(d) compares the voltage distribution at different nodes of the grid under different optimization objectives. It can be observed that when minimizing grid losses, (J_1) is the optimization objective and the grid voltage approaches 1.21, which is the square of the reference voltage of 110%. Under other methods, the grid voltage remains close to the reference value, indicating better control effectiveness.

4.3. Analysis and Discussion. To analyze the impact of different deviation metrics on the optimization results, Table 6 presents the optimization results of the multienergy system under different norm forms. In this table, the infinity norm measures the maximum allowable deviation, the two norm measures the sum of squared deviations, and the one norm measures the sum of absolute deviations. From the comparison results presented in Table 6, it can be observed that under different norms, the variation in objective function values is small, and there is no dominance among the optimization results for different norms. This indicates that the optimization results under different norms are all non-dominant solutions of multiobjective optimization, and the optimization results are not sensitive to the norm definition.

In the multienergy system, to reflect the bias towards different optimization objectives in the actual application process, this paper introduces weight coefficients for different optimization objectives in equation (5), as shown in equation (6), where ω_s represents the weight coefficient for

Table 6: Comparison of optimization results of different metric functions for tolerance.

	J_1	J_2	J_3	J_4	r_1	r_2	r_3	r_4
Expectation point	0.0294	0.0027	−9.5580	11584.3200	—	—	—	—
$\|r\|_\infty$	0.0700	0.0063	−9.5347	27581.8172	1.3810	1.3810	1.3810	1.3810
$\|r\|_2$	0.0654	0.0062	−9.3551	28413.7869	1.2231	1.3121	0.0212	1.4528
$\|r\|_1$	0.0637	0.0063	−9.3722	28407.4498	1.1661	1.3686	0.0195	1.4522

the allowable deviation of the s-th optimization objective. To further discuss the impact of weight coefficient variations on the optimization results, Table 7 presents the optimization results of the multienergy system under different weight combinations for the four optimization objectives.

$$\begin{aligned} &\text{minimize} \max\left(r_1, r_2, \ldots, r_S\right) = \|\mathbf{r}\|_2^2 \\ &\text{Subject to} \begin{cases} g_k(\mathbf{X}) \le 0, k = 1, 2, \ldots, K, \\ h_l(\mathbf{X}) \le 0, l = 1, 2, \ldots, L, \\ x_i^{\text{lb}} \le x_i \le x_i^{\text{ub}}, i = 1, 2, \ldots, m, \\ f_s(\mathbf{X}) \le \dfrac{\omega_s}{\sum_{j=1}^{S} \omega_j} r_s \left|\min\left(f_s(\mathbf{X})\right)\right| + \min\left(f_s(\mathbf{X})\right). \end{cases} \end{aligned} \tag{6}$$

From Table 7, it can be observed that under the condition of weight variation for ω_1 to ω_3, as the weight value ω_1 decreases, the allowable deviation of the objective function J_4 decreases. This means that the optimization result is closer to the desired value on the J_4 objective. By reducing the weight coefficient of a specific optimization objective, the allowable deviation for that objective can be controlled, thereby achieving a preference for a specific optimization objective. At the same time, there are some differences in the variation patterns of the objective values under the condition of equal weights for the other three objectives. The objective J_3 shows the greatest improvement when ω_4 changes from 7 to 1, while J_1 and J_2 show the greatest improvement when ω_4 changes from 0.1 to 0.01. This indicates that different optimization objectives have different sensitivities to the weights, and therefore, it is necessary to conduct further discussions. Figure 6 shows the variation curves of the four objective values under different weight variations for the optimization objectives. It should be noted that the weights of the other three objectives change in equal increments along the x-axis, representing the weight of the optimization objective.

In Figure 6(a), it can be observed that under the condition of equal values for ω_2 to ω_4, as the weight ω_1 increases, the objective value J_1 shows an exponential growth trend. Before $\omega_1 = 0.7$, the growth is relatively slow, but after $\omega_1 = 0.7$, it increases rapidly. On the other hand, the objective value J_2 experiences a sudden drop and then remains unchanged, indicating that J_2 is not sensitive to the variation of ω_1. Objective values J_3 and J_4 have a plateau period, and after this period, J_3 increases while J_4 decreases. The increase in J_3 implies an increase in the abandonment of renewable energy, which is due to the decrease in weight ω_4 caused by the increase in ω_1, indicating that the optimization objective J_2 is given higher priority, thus affecting the integration of renewable energy. Similarly, from Figure 6(b), it can be observed that under the condition of equal values for ω_1, ω_3, and ω_4, as the weight ω_2 increases, the objective value J_2 shows an exponential growth trend. Before $\omega_2 = 0.9$, the growth is relatively slow, but after $\omega_2 = 0.9$, it increases rapidly. On the other hand, the objective values J_1, J_3, and J_4 gradually decrease and enter a plateau phase. This indicates that J_1, J_3, and J_4 are only influenced by ω_2 within a certain range. In Figure 6(c), under the condition of equal values for ω_1, ω_2, and ω_4, as the weight ω_3 increases, all the objective values J_1 to J_4 show rapid changes and then tend to stabilize. Simultaneously, as the abandonment of renewable energy increases, the objective value J_3, which represents voltage fluctuations in the grid, decreases. However, the system network losses and operation costs increase. Nevertheless, the changes in the objective values J_1, J_2, and J_4 are very small. This implies that the impact of allowable deviation of the optimization objective J_3 on the optimization results can be almost negligible. In Figure 6(d), under the condition of equal values for ω_1 to ω_3, as the weight ω_4 increases, the objective values J_3 and J_4 gradually increase. This means that as the system operating costs are relaxed, the abandonment of renewable energy will increase continuously. At the same time, the objective J_1, which represents network losses, decreases rapidly, and the voltage fluctuations in the grid decrease slowly, but the numerical changes are small. This indicates that the system operating costs have a significant

Table 7: Comparison of optimization results for different weights of tolerance.

ω_1	ω_2	ω_3	ω_4	$\min \|r\|_2^2$	J_1	J_2	J_3	J_4
1	1	1	7	0.0498	0.0045	−7.1911	67894.6029	
1	1	1	1	0.0700	0.0063	−9.5347	27581.8172	
1	1	1	0.1	0.3383	0.0307	−9.5580	23751.0729	
1	1	1	0.01	1.2602	0.1137	−9.5580	16432.1650	

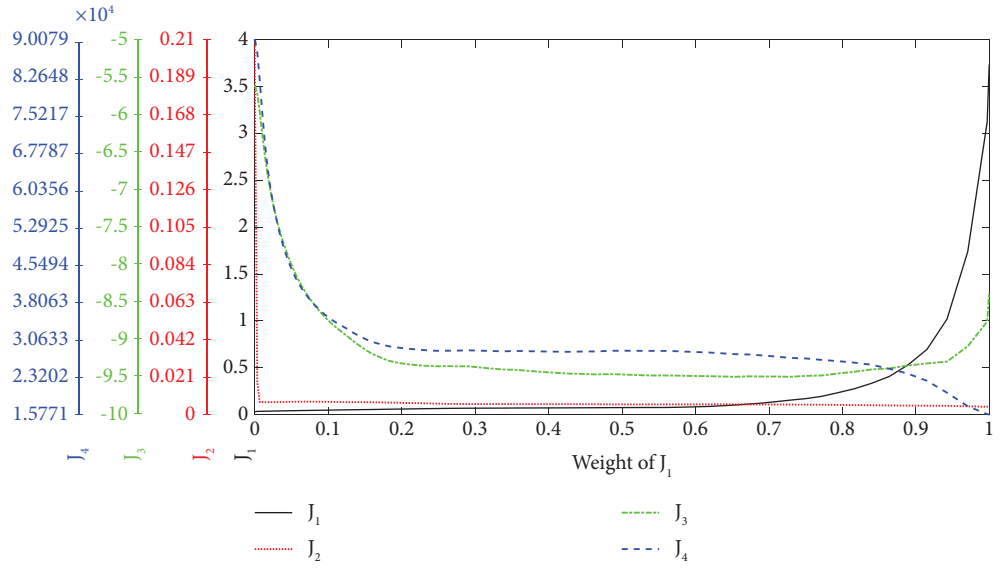

(a)

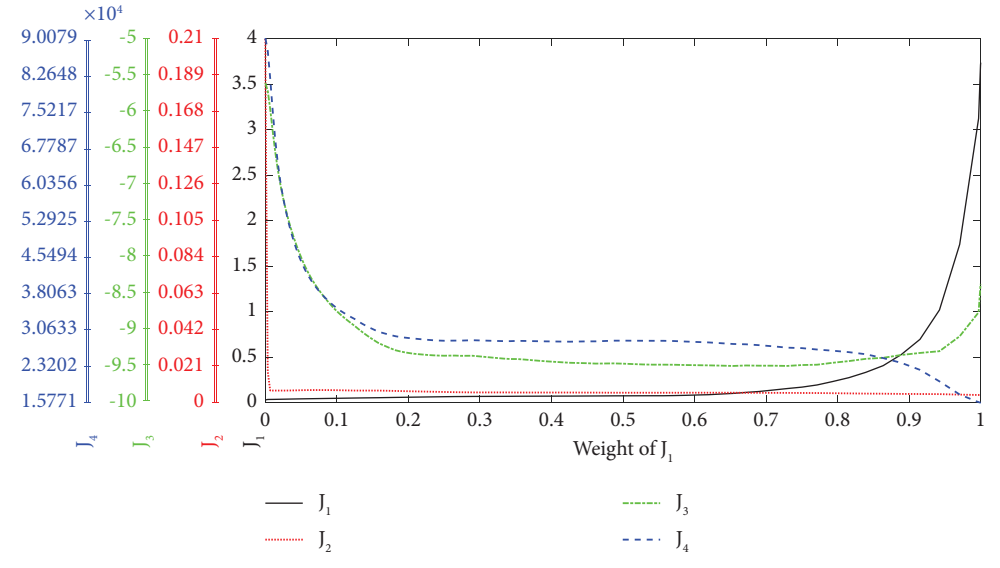

(b)

Figure 6: Continued.

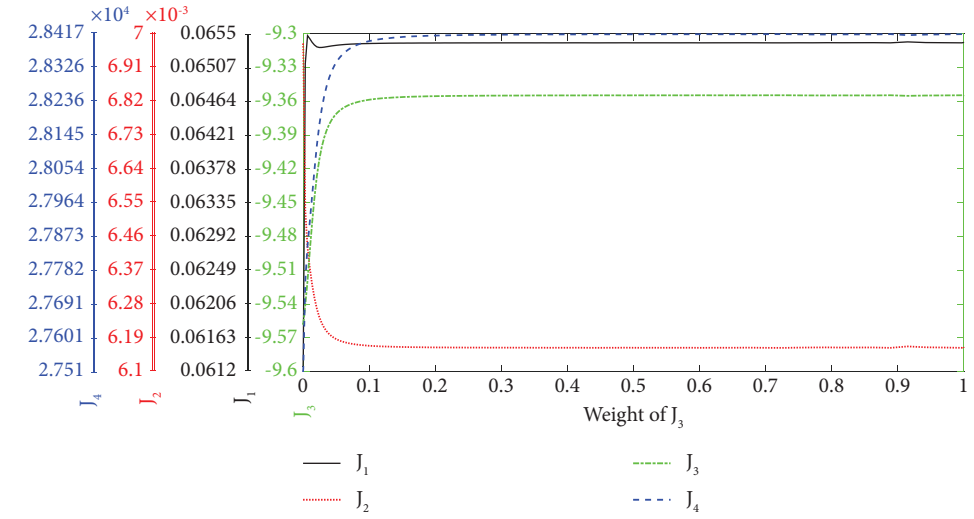

(c)

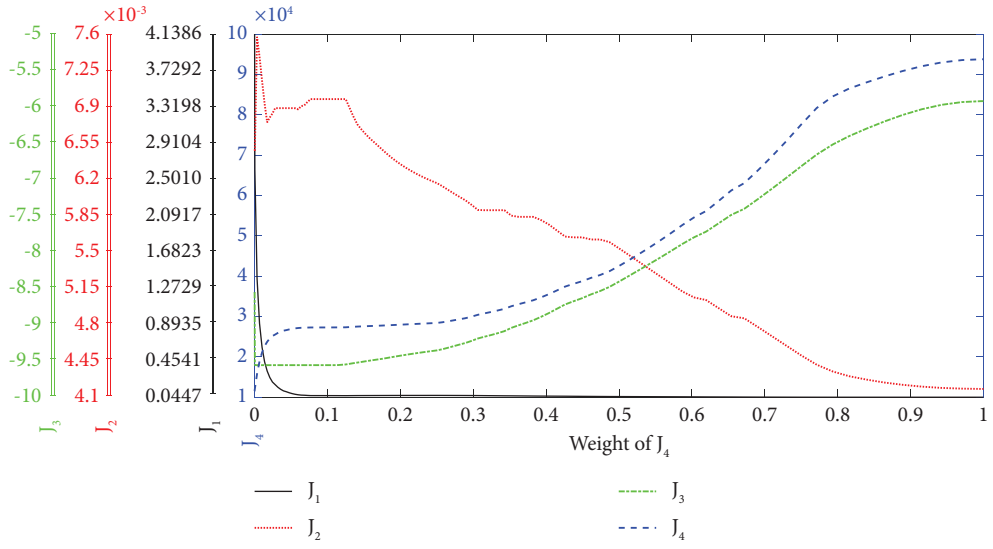

(d)

Figure 6: The variation curve of each optimization objective value under the variation of tolerance weight for different optimization objectives. (a) Optimization result curve under tolerance weight change of objective function J_1. (b) Optimization result curve under tolerance weight change of objective function J_2. (c) Optimization result curve under tolerance weight change of objective function J_3. (d) Optimization result curve under tolerance weight change of objective function J_4.

impact on network losses within a small range, while their effect on grid voltage is minimal. From the above analysis, it can be concluded that there is a complex coupling relationship among the optimization objectives in the multienergy system. Simply modifying the weight of a single optimization objective may have a minimal impact on the overall optimization results or even cause step changes. Therefore, the coupling relationships and sensitivities among the optimization variables will be one of the important research topics in subsequent multiobjective optimization calculations.

In order to present the optimization results of the proposed method more intuitively, we take the example of a two-objective optimization consisting of objective functions J_1 and J_4 and analyze the position of the obtained optimization results on the Pareto frontier as shown in Figure 7.

In Figure 7, it can be seen that in the optimization model with objective functions J_1 and J_4, the coordinates of the expected point A are $(0.0294,\ 1.158\times10^4)$, and the coordinates of the optimal point B obtained by the proposed method are $(0.04528,\ 2.752\times10^4)$. The optimal point B is located on the Pareto frontier of the two-objective optimization model, indicating that the optimization results are effective. Moreover, from the shape of the Pareto frontier, when the optimization objective J_1 increases, the optimization objective J_4 first decreases rapidly, then decreases slowly, and finally approaches the corresponding ordinate

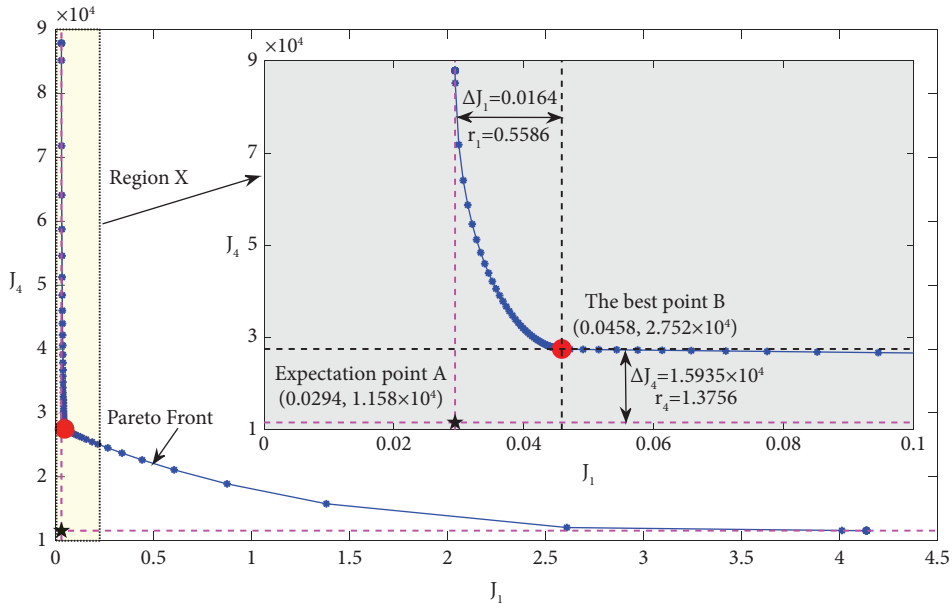

Figure 7: The position of optimization results on the Pareto front in two objective functions J_1 and J_4 example.

value of the expected point. This means that under the condition of sacrificing the optimization objective J_1, the optimization objective J_4 gains rapidly and then levels off. The optimal point obtained by the proposed method is exactly at the point where the optimization objective J_4 starts to decrease rapidly, indicating that the proposed method balances the overall benefits of the two optimization objectives and is superior. Furthermore, the tolerances on J_1 and J_4 are $r_1 = 0.5586$ and $r_4 = 1.3756$, respectively, and it is evident that r_4 is greater than r_1. This means that the multienergy system requires a higher tolerance level for the optimization objective J_4. More specifically, if the tolerance for the optimization objective J_4 is reduced and the allowable deviation is reduced, the cost required for the multienergy system to achieve the optimization objective J_1 will be higher.

5. Conclusion

To address the problem of multiservice objective optimization in multienergy systems, a two-stage optimization framework and method based on the expected point tolerance are proposed in this paper. Based on the expected point derived from the optimization results of each single objective function, the characteristic of the proposed method is to transform a multiobjective optimization problem into a single optimization objective solution by describing the distance between the nondominated solutions on the Pareto frontier and the expected point. In the IEEE 33-bus simulation example including a multienergy system, the comparative results and analysis conclusions have been as follows. Compared with the optimal results under each single objective method, the proposed method increases power line loss, maximum voltage deviation, new energy consumption, and economy by 2.22, 2.30, 1.02, and 2.45 times, respectively. Compared with the suboptimal results, the proposed method reduces power line loss by 22.26, 1.74, 1.09, and 0.97 times, respectively. The proposed method can effectively balance the contradictions between different optimization objectives and ensure that the optimization results are more reasonable. Under different deviation metrics of the proposed method, the maximum relative errors on each objective function are 9.0%, 1.59%, 1.88%, and 2.93%, respectively. This indicates that the optimization results under different norms are all nondominant solutions of multiobjective optimization, and the optimization results are not sensitive to the norm definition. It means that the impact of different deviation metrics on optimization results is relatively small. Based on the comparison results of tolerance weights for different objective functions, there is a complex coupling relationship between the optimization objectives, and the impact of a tolerance weight on the optimization results is significant. Therefore, the coupling relationship and sensitivity analysis among optimization objectives will be the important topics in future research.

Data Availability

The data used to support the findings of this study are available from the corresponding author upon request. Also, Figures 2 and 3 used to support the findings of this study are reproduced from the below literature, [34].

Conflicts of Interest

The authors declare that they have no conflicts of interest.

Acknowledgments

This study was sponsored by Beijing Nova Program (Z211100002121081) Research start-up fund of North China University of Technology (110051360023XN224-22).

References

[1] Q. Li, J. Wang, J. Chen, T. Ding, and C. Gu, "A hierarchical multi-area capacity planning model considering configuration ratios of renewable energy and energy storage systems with multi-area coordination," *IET Generation, Transmission & Distribution*, vol. 17, no. 16, pp. 3658–3677, 2023.

[2] C. Gu, J. Wang, Y. Zhang, Q. Li, and Y. Chen, "Optimal energy storage planning for stacked benefits in power distribution network," *Renewable Energy*, vol. 195, pp. 366–380, 2022.

[3] H. Zuo, Y. Teng, S. Cheng, P. Sun, and Z. Chen, "Distributed multi-energy storage cooperative optimization control method for power grid voltage stability enhancement," *Electric Power Systems Research*, vol. 216, Article ID 109012, 2023.

[4] S. Ma, Y. Wu, L. Jianlin, J. Xiong, and W. Zeng, "Research on optimal configuration of centralized battery energy storage for multiple service objectives," *High Voltage Apparatus*, vol. 59, no. 07, pp. 75–86, 2023.

[5] T. Cheng, M. Chen, Y. Wang et al., "Adaptive robust method for dynamic economic emission dispatch incorporating renewable energy and energy storage," *Complexity*, vol. 2018, Article ID 2517987, 13 pages, 2018.

[6] H. Di, Y. Xin, G. Lin, C. Zhang, and H. Chen, "Interval economic dispatch of multi-objective cooperative game considering wind power and energy storage connected to power grid," *Control Theory & Applications*, vol. 38, no. 07, pp. 1061–1070, 2021.

[7] M. Lu, J. Guan, H. Wu et al., "Day-ahead optimal dispatching of multi-source power system," *Renewable Energy*, vol. 183, pp. 435–446, 2022.

[8] L. Uwineza, H. G. Kim, J. Kleissl, and C. K. Kim, "Technical control and optimal dispatch strategy for a hybrid energy system," *Energies*, vol. 15, no. 8, p. 2744, 2022.

[9] M. R. Sandgani and S. Sirouspour, "Coordinated optimal dispatch of energy storage in a network of grid-connected microgrids," *IEEE Transactions on Sustainable Energy*, vol. 8, no. 3, pp. 1166–1176, 2017.

[10] M. Premkumar, R. Sowmya, C. Ramakrishnan et al., "An efficient and reliable scheduling algorithm for unit commitment scheme in microgrid systems using enhanced mixed integer particle swarm optimizer considering uncertainties," *Energy Reports*, vol. 9, pp. 1029–1053, 2023.

[11] C. Ji, C. Zhong, K. Li, M. Xu, J. Shao, and F. Zheng, "Research on multiple objection operation strategy optimization of distribution network including distributed energy storage," in *Proceedings of the 2017 4th International Conference on Information Science and Control Engineering (ICISCE)*, pp. 1163–1167, Changsha, China, July 2017.

[12] M. Purlu and B. E. Turkay, "Optimal allocation of renewable distributed generations using heuristic methods to minimize annual energy losses and voltage deviation index," *IEEE Access*, vol. 10, pp. 21455–21474, 2022.

[13] Y. Liu, Q. Liu, H. Guan et al., "Optimization strategy of configuration and scheduling for user-side energy storage," *Electronics*, vol. 11, no. 1, p. 120, 2021.

[14] J. Sun, Z. Li, J. Li, G. Wu, and Y. Xia, "Hybrid power system with adaptive adjustment of weight coefficients multi-objective model predictive control," *International Journal of Electrical Power & Energy Systems*, vol. 153, Article ID 109296, 2023.

[15] L. Li, P. Liu, Z. Li, and X. Wang, "A multi-objective optimization approach for selection of energy storage systems," *Computers & Chemical Engineering*, vol. 115, pp. 213–225, 2018.

[16] T. Terlouw, P. Gabrielli, T. AlSkaif, C. Bauer, R. McKenna, and M. Mazzotti, "Optimal economic and environmental design of multi-energy systems," *Applied Energy*, vol. 347, Article ID 121374, 2023.

[17] W. Fan, Q. Tan, A. Zhang et al., "A Bi-level optimization model of integrated energy system considering wind power uncertainty," *Renewable Energy*, vol. 202, pp. 973–991, 2023.

[18] N. Pourghaderi, M. Fotuhi-Firuzabad, M. Moeini-Aghtaie, M. Kabirifar, and M. Lehtonen, "Optimal energy and flexibility self-scheduling of a technical virtual power plant under uncertainty: a two-stage adaptive robust approach," *IET Generation, Transmission & Distribution*, vol. 17, no. 17, pp. 3828–3847, 2023.

[19] Y. Qiu, Q. Li, Y. Ai et al., "Two-stage distributionally robust optimization-based coordinated scheduling of integrated energy system with electricity-hydrogen hybrid energy storage," *Protection and Control of Modern Power Systems*, vol. 8, no. 1, p. 33, 2023.

[20] Y. Luo, Y. Gao, and D. Fan, "Real-time demand response strategy base on price and incentive considering multi-energy in smart grid: a bi-level optimization method," *International Journal of Electrical Power & Energy Systems*, vol. 153, Article ID 109354, 2023.

[21] Y. Zhang, K. Zhong, W. Deng et al., "An optimal scheduling of renewable energy in flexible interconnected distribution networks considering extreme scenarios," *IET Renewable Power Generation*, vol. 17, no. 10, pp. 2531–2541, 2023.

[22] H. Yang, J. Wu, and X. Du, "Thermo-economic analysis and multi-objective optimization of solar aided pumped thermal electricity storage system," *Journal of Energy Storage*, vol. 70, Article ID 107994, 2023.

[23] X. Wu, B. Liao, Y. Su, and S. Li, "Multi-objective and multi-algorithm operation optimization of integrated energy system considering ground source energy and solar energy," *International Journal of Electrical Power & Energy Systems*, vol. 144, Article ID 108529, 2023.

[24] D. Sagawa and K. Tanaka, "Machine learning-based estimation of COP and multi-objective optimization of operation strategy for heat source considering electricity cost and on-site consumption of renewable energy," *Energies*, vol. 16, no. 13, p. 4893, 2023.

[25] A. Mishra, B. B. Arora, and A. Arora, "Multi-objective optimization of an inlet air-cooled combined cycle power plant," *Journal of Thermal Science and Engineering Applications*, vol. 15, no. 7, Article ID 071005, 2023.

[26] X. Liao, B. Qian, Z. Jiang, B. Fu, and H. He, "Integrated energy station optimal dispatching using a novel many-objective optimization algorithm based on multiple update strategies," *Energies*, vol. 16, no. 13, p. 5216, 2023.

[27] G. Fan, Z. Liu, X. Liu et al., "Energy management strategies and multi-objective optimization of a near-zero energy community energy supply system combined with hybrid energy storage," *Sustainable Cities and Society*, vol. 83, Article ID 103970, 2022.

[28] Z. Liu, Z. Xiao, Y. Wu et al., "Integrated optimal dispatching strategy considering power generation and consumption interaction," *IEEE Access*, vol. 9, pp. 1338–1349, 2021.

[29] A. Reza, S. Mojtaba, and D. W. Philip, "A flexibility-based multi-objective model for contingency-constrained transmission expansion planning incorporating large-scale hydrogen/compressed-air energy storage systems and wind/solar farms," *Journal of Energy Storage*, vol. 70, 2023.

[30] G. Ma, J. Li, and X. P. Zhang, "Energy storage capacity optimization for improving the autonomy of grid-connected microgrid," *IEEE Transactions on Smart Grid*, vol. 14, no. 4, pp. 2921–2933, 2023.

[31] Y. Chen, L. Feng, X. Li, M. Zoghi, and K. Javaherdeh, "Exergy-economic analysis and multi-objective optimization of a multi-generation system based on efficient waste heat recovery of combined wind turbine and compressed CO_2 energy storage system," *Sustainable Cities and Society*, vol. 96, Article ID 104714, 2023.

[32] B. Ahmadi, O. Ceylan, A. Ozdemir, and M. Fotuhi-Firuzabad, "A multi-objective framework for distributed energy resources planning and storage management," *Applied Energy*, vol. 314, Article ID 118887, 2022.

[33] L. Yibing, W. Wenchuan, Z. Boming, L. Zhengshuo, and J. Yuntao, "Reactive power optimization for three-phase distribution networks with distributed generators based on mixed integer second-order cone programming," *Automation of Electric Power Systems*, vol. 38, no. 15, pp. 58–64, 2014.

[34] S. Ma, Y. Wu, Y. Jiang, Y. Li, and G. Sha, "Research on two-stage optimization control method for energy storage systems based on multi service attribute utility evaluation," *Energy Sources, Part A: Recovery, Utilization, and Environmental Effects*, vol. 46, no. 1, pp. 3041–3060, 2024.